GL03100-3 of 4

JOURNAL OF GEOPHYSICAL RESEARCH, VOL. 90, NO. B1, PAGES 745–758, JANUARY 10, 1985

The Heber Geothermal Field, California: Natural State and Exploitation Modeling Studies

MARCELO J. LIPPMANN AND GUDMUNDUR S. BODVARSSON

Earth Sciences Division, Lawrence Berkeley Laboratory, University of California

Using numerical simulation techniques and an axisymmetric model of the Heber geothermal field, the natural (preexploitation) state of the system and its response to fluid production are analyzed. The results of the study indicate that the Heber geothermal anomaly is sustained by the upflow of hot water through a central zone of relatively high permeability. The best model suggests that in its natural state the system is recharged at depth by a 15-MW_t (megawatts thermal) (reference temperature 0°C) convective heat source. The existence of an axisymmetric convection pattern, whose axis coincides with the center of the Heber anomaly, is also suggested. At the lower part of the ascending hot water plume the deep recharge water mixes with colder water moving laterally toward the axis of the system. In the upper part the rising plume spreads radially outward after reaching the bottom of the cap rock, at about 550 m depth. The model results suggest that the so-called cap rock is quite permeable (5×10^{-15} m^2) with convection controlling its temperature distribution. The results also show reduced permeability (10×10^{-15} m^2) of the upper zones in the outer region of the system that may be due to mineral precipitation. In modeling the exploitation of the field the generation rate is allowed to build up over a period of 10 years; after that, 30 years of constant power production is assumed. Full (100%) injection of the spent brines is considered; the fluids being injected 2250 m ("near injection") or 4250 m ("far injection") from the center of the system. The study shows that a maximum of 6000 kg/s (equivalent to approximately 300 MW_e (megawatts electric)) of fluids may be produced for the near injection case but only 3000 kg/s (equivalent to approximately 150 MW_e) for the far injection case. The results indicate that the possible extraction rates (generating capacity) are generally limited by the pressure drop in the reservoir. The average temperature of the produced fluids will decline 10°–18°C over the 40-year period.

INTRODUCTION

The Heber geothermal field is located in the southern part of the Imperial Valley, California, about 7 km north of the Mexican border (Figure 1). In the 1970's exploration drilling, mainly by Chevron Geothermal Co. and Union Geothermal Co., delineated this moderate-temperature (<200°C), liquid-dominated geothermal system. Chevron Geothermal Co., the operator of the field, estimates that the Heber system can support a power generation of 500 MW_e (megawatts electric) for at least 30 years [*Salveson and Cooper*, 1981; *California Division of Oil and Gas*, 1983*a*].

Construction of the first two power plants (a 45-MW_e (net) binary plant and a 47-MW_e (net) dual-flash plant) has recently begun. The plants are scheduled to be completed in mid-1985. The production and injection wells for the two projects are being drilled directionally from drilling "islands." Initially, 13 production and nine injection wells are proposed for the binary plant, and nine production and eight injection wells for the dual-flash plant [*California Division of Oil and Gas*, 1983*b*].

In late 1980, San Diego Gas and Electric Company and the Department of Energy (DOE) signed a cooperative agreement calling for DOE to share in the cost of the Heber Geothermal Binary Demonstration Project [*Allen and Nelson*, 1983]. The purpose of our work at Lawrence Berkeley Laboratory, as advisors to DOE, is to study carefully the response of the field to exploitation and identify potential reservoir problems at Heber. For example, excessive reservoir pressure declines can seriously affect the economics of the project since the Heber wells must be pumped, owing to the low reservoir temperature. Also, the limited size of the thermal anomaly could result in rapid fluid temperature decline during production, which would greatly reduce the efficiency of the heat exchangers. Consequently, one should carefully evaluate the reservoir behavior under different exploitation schemes.

In the present paper we use numerical modeling techniques to study the reservoir response to exploitation. However, before modeling the production period, one must fully understand its natural behavior (before exploitation), the mass and energy fluxes in the system, and the boundary conditions that apply. Thus, in the first part of the paper we develop a coarse model of the natural state of the Heber geothermal field and calculate steady state mass and heat flows through the system. The resulting temperatures and pressures in the model are compared to field observations. Using a two-dimensional axisymmetric model, we are able to match temperature and pressure data from the field reasonably well. Then the computed temperature and pressure distributions and the boundary conditions determined by the natural state model are used to evaluate the generating capacity of the Heber system under different production-injection scenarios.

AVAILABLE DATA

Relatively little information has been published on the subsurface characteristics of the Heber geothermal system. According to *Tansev and Wasserman* [1978] this approximately circular geothermal area is characterized by high heat flow, an electrical resistivity low, and a positive gravity anomaly; there are no surface manifestations in the field.

The exploration and development of Heber has been summarized by *Salveson and Cooper* [1981]. The first well at Heber was drilled in 1945 by Amerada. In 1963, Chevron drilled a shallow test hole that confirmed the geothermal anomaly [*Butler*, 1975]. During the 1970's, additional explora-

Paper number 4B5058.
0148-0227/85/004B-5058$05.00

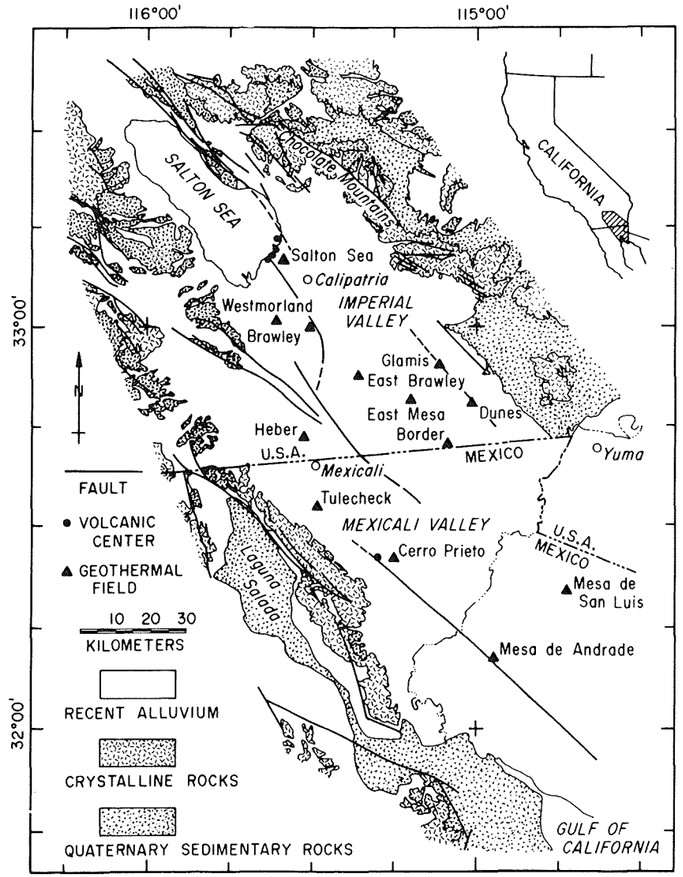

Fig. 1. Location of geothermal areas in the Salton Trough [from *Elders and Cohen*, 1983].

tion wells were drilled that delineated the geothermal reservoir (Figure 2). These wells, ranging in depth from 1000 to over 3000 m, helped characterize the subsurface geology of the area. Development drilling started in 1982 and is still continuing [*California Division of Oil and Gas*, 1983*b*].

Tansev and Wasserman [1978] describe the Heber field as part of the Colorado River deltaic environment consisting of interbedded sandstones and shales. The shales are thick and predominant to about 610 m depth; below that, sandstone layers prevail, and the shale layers become thinner. From about 2400 to 3000 m, sandstones are predominant with minor shale breaks. The hydrologic continuity of several sandstone layers has been confirmed by well tests. A few faults have been identified, but according to Tansev and Wasserman, any faults present in the more sandy section would not significantly hamper fluid flow; they could even enhance it. Measurements in Heber wells indicate that the pressure gradient in the reservoir is approximately 9.5 MPa/km, which is the hydrostatic pressure gradient for 170°C liquid water. The near-radial distribution of temperature in the system suggests upflow from depth in the center of the anomaly.

Salveson and Cooper [1981] show that temperature data from Heber wells outline a convective plume of hot water of 190°C temperature, or higher, rising from depths below 3000 m. Above 1350 m, horizontal fluid flow shifts the plume northerly. The hot plume centers near well Nowlin 1 at about 600 m depth but is displaced about 800 m toward the south at 1200 m depth (Figure 3). Salveson and Cooper state that the cap rock (predominantly shales) at Heber extends down to a depth of 600 m with intergranular porosities of 15–30%. To our knowledge, no other values of reservoir parameters at Heber have been published.

The heat source at Heber has not been identified. At least two of the wells (Holtz 1 and Nowlin 1) intersected igneous dikes; only data on the cuttings of Holtz 1 have been published. This well penetrated a diabase dike or sill, probably of Pleistocene age, at a depth of 1335–1366 m. However, such a small rock body could not be the sole heat source for the present Heber geothermal anomaly [*Browne*, 1977]. On the basis of the shape of the isotherms at shallow depths it can be postulated that the Heber field is fed by a relatively permeable zone, perhaps a fault (or intersection of two or more faults). This has been suggested to be the case at the nearby East Mesa field [*Riney et al.*, 1980; *Goyal and Kassoy*, 1981]. However, it is difficult to confirm this hypothesis since a fault map for Heber has not been published.

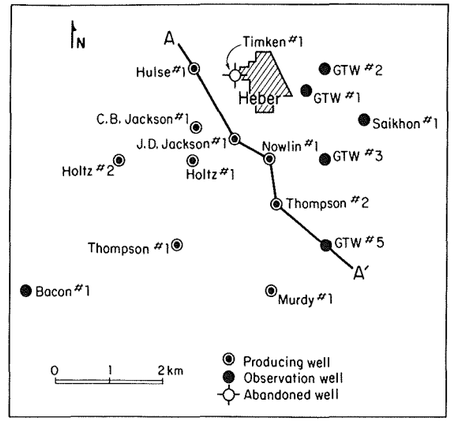

Fig. 2. Heber. Location of pre-1979 wells and cross section shown on Figure 3 (modified from *Salveson and Cooper* [1981]).

Mineralogical studies of well cuttings from a single well, Holtz 1 [*Browne*, 1977], indicate that temperatures have changed in the field during its evolution. Fluid inclusion data indicate that at least locally, the reservoir has been cooling at an undetermined rate, from a maximum temperature of 240°C, and that there were at least two significant pulses of hot fluids in this well.

Tansev and Wasserman [1978] reported that Chevron plans to develop a nearly circular 30.3 km^2 area with each plant increment representing a sector of the circle. *Salveson and Cooper* [1981] indicated that the wells were to be directionally drilled for production from surface islands into the high-temperature part of the thermal anomaly. Bottom hole locations were to be evenly distributed in a circular pattern having a radius of about 600 m.

The power plants will be located near the producing islands to minimize heat loss during the transmission of the hot fluid at the surface; the two power plants presently under construction are about 1.5 km apart. The spent brine will be piped from the power plants to injection islands on the periphery of the field. There, 2.4–4.0 km from the center of the anomaly, the brine will be reinjected through directionally drilled wells.

For the production depth of 600–1800 m assumed by *Tansev and Wasserman* [1978], 2.28 m^3/s of fluid will initially be required to generate 100 MW$_e$. For a fluid density of 900 kg/m^3 this would correspond to about 2050 kg/s. Later as the temperature of the produced fluids declines, the required production rate will increase. *Allen and Nelson* [1983, Figure 1] state that 970 kg/s of geothermal fluids are needed for the 45-MW$_e$ (net) binary plant. For the 47-MW$_e$ (net) dual-flash plant, *De Haven* [1982] mentions a rate of about 1020 kg/s. In other words, about 1000 kg/s of fluid will be required to generate 50 MW of electrical power.

All fluids produced from the reservoir will be reinjected; because of losses, some makeup waters from surface sources will be required. For the binary plant the temperature of the injected fluids will be 72.2°C [*Allen and Nelson*, 1983, Figure 1] and about 93°C for the binary plant and the dual-flash plant, respectively.

PREVIOUS RESERVOIR MODELING WORK

The only published reservoir modeling study of the Heber system under production is that by *Tansev and Wasserman* [1978]. They use a three-dimensional, single-phase (liquid) nonisothermal simulator. Their model of the geothermal reservoir covers a 30.3 km^2 area and consists of two main zones; zone 1, from 600 to 1200 m (2000 to 4000 ft) depth, and zone 2, from 1200 to 1800 m (4000 to 6000 ft) depth. Zone 1 is subdivided into 15 horizontal sandstone and shale layers and zone 2 into 113 layers. The model is further divided into eight sectors each consisting of 15 rows.

Tansev and Wasserman [1978] assumed that (1) the sandstones and shale layers are continuous, homogeneous, and isotropic, (2) the initial temperatures vary only as a function of radial coordinate and do not vary vertically in a given zone, (3) the regional groundwater movement is negligible, (4) no heat (or mass) recharge occurs from the underlying strata (below 1800 m), and (5) (in most cases studied) no cross flow exists between the sectors. No data are given regarding thermal and hydraulic properties assigned to the different layers.

Fluids are assumed to be produced from both zones (between 600 and 1800 m depth) to sustain a constant 200-MW$_e$ total generating capacity. Hot fluids are extracted near the axis of the system, and the spent brine is reinjected near its periphery (the exact locations are not given). The initial total fluid production rate is 4.56 m^3/s, but as the temperature of the produced fluids decreases, the production rate increases. Some of the conclusions reached by *Tansev and Wasserman* [1978] are that (1) both zones show a 16.7°C temperature

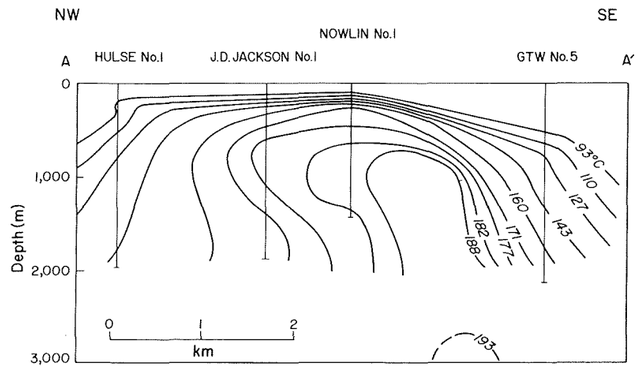

Fig. 3. Temperature distribution in the Heber geothermal field (modified from *Salveson and Cooper* [1981].

decline over a 30-year production period, (2) the Heber system between 600 and 1800 m (zones 1 and 2) alone can support 250 MW_e power production, and (3) in general, the generating capacity of Heber will be restricted mainly by the pressure drop rather than by the temperature decline (a temperature of 160°C for the power plant is assumed as an economic cutoff point).

Although the *Tansev and Wasserman* [1978] model seems to give a reasonable evaluation of the Heber reservoir, we felt another model should be developed that matches well the natural state of the system. Our experience in modeling geothermal fields has shown the importance of fully understanding the natural state of the system before simulating its response to exploitation. In modeling the natural state one does not only obtain initial conditions for the exploitation modeling but also gains insight into the mass and heat flow through the system and its hydrological and thermal parameters. An additional motivation for this modeling study of Heber is the fact that available information on the model developed by *Tansev and Wasserman* [1978] is incomplete.

METHODOLOGY

In the present work we use the numerical simulator PT [*Bodvarsson*, 1982] that is capable of modeling three-dimensional mass and energy transport in fully saturated fractured and/or porous media rocks. It employs the "integrated finite difference method" for discretizing the medium and formulating the governing equations [*Edwards*, 1972]. The set of linear equations is solved at each time step by direct means using an efficient sparse matrix solver [*Duff*, 1977]. The simulator is quite general, as it allows for temperature- and/or pressure-dependent fluid and rock properties. The fluid density is calculated as a function of pressure and temperature, using a polynomial approximation that is accurate to within 1%. Fluid viscosity is calculated as a function of temperature using an accurate (within 1%) exponential expression. The simulator has been validated against many analytical solutions as well as field experiments [*Doughty et al.*, 1983]. A detailed description of the simulator is given by *Bodvarsson* [1982].

For both the natural state and exploitation studies we use a multilayered axisymmetric model. We do not model individual layers of sandstone and shale, as the data publicly available are not detailed enough. Instead, we model the system as homogeneous anisotropic media. This simplification may not make the model appropriate to study the breakthrough of the injected water in the production area.

In modeling the natural (preexploitation) state of the system we assume that it is under steady state conditions and neglect the gradual cooling of the reservoir, as indicated by mineralogic studies [*Browne*, 1977]. The temperatures and pressures at the boundaries, the rock properties of the different zones in the model, and the amount of hot water recharging the system under natural conditions are varied in order to match the computed values with the pressure gradient indicated by *Tansev and Wasserman* [1978], i.e., 9.5 MPa/km, and the temperature distribution given by *Salveson and Cooper* [1981], see Figure 3.

The initial and boundary conditions for modeling the Heber reservoir under exploitation correspond to that of the natural state model. The change of reservoir pressures and the average temperature of the produced fluids for different assumed development plans are the main parameters used to establish the feasibility of the fluid production-injection schemes considered in this study.

DESCRIPTION OF THE MODEL

In the simulations we use a multilayered axisymmetric model. The outer radial boundary, 10 km from the axis, is assumed to be open to heat and mass flow. The temperatures at this boundary are assumed to increase linearly with depth following a geothermal gradient (around 50°C/km); the pressures are hydrostatic for the assumed vertical temperature distribution.

The top boundary, corresponding to ground surface level, is considered open only to heat flow; it is kept at a constant temperature of 22°C (the mean annual temperature in the area [*Imperial Irrigation District*, 1978]). The bottom boundary of the model is placed at a sufficient depth (4950 m) to allow the development of a fluid circulation pattern that reproduces the temperature distribution observed in the upper 3000 m of the reservoir (Figure 3). This boundary does not correspond to a given geologic/geophysical surface. Seismic refraction data suggest that in the general area of the Heber field the sedimentary section is at least 4 km deep. However, the lack of perceptible reflections from a sedimentary/basement suggests a gradual metamorphic change [*Fuis et al.*, 1984]. The bottom boundary is postulated to have a constant temperature, computed from the assumed geothermal gradient and surface temperature. An upflow zone feeding hot water to the reservoir system is assumed to exist over a 1000-m radius at the bottom of the reservoir system. The amount and temperature of the fluids recharging the system through the upflow zone are varied during the simulations. The remainder of the bottom boundary is closed to fluid flow. The geothermal gradient was changed during the simulations to agree with the assumed temperature of the upflow fluids at 4950 m depth.

The model is divided into five zones with different rock properties, primarily different permeability values (Figure 4). Zones 1 and 2 are 550 m thick and represent the cap rock. Zone 3, representing a cylinder of 1000 m radius, is the hot water upflow zone. Zones 4 and 5 correspond to the outer regions of the field.

MODELING OF THE NATURAL STATE

The modeling of a geothermal system in its natural state is a necessary step before simulations of field performance under exploitation are carried out. This type of modeling effort is time consuming, as many iterations are needed before a reasonable match with observed data is achieved. However, the information contained in the natural thermodynamic conditions of a field can, if properly analyzed, help determine the permeability distribution in the field and the natural mass and heat recharge; parameters that can greatly affect the response of the geothermal system to full-scale exploitation. Detailed numerical natural state modeling studies have been reported by *Lippmann and Bodvarsson* [1983*a*] on the Cerro Prieto geothermal field, Mexico, and *Bodvarsson et al.* [1982, 1984] on the Krafla geothermal field in Iceland.

Model Parameters

Several models with different rock properties, boundary conditions, and heat source strength were analyzed, and the results were compared to the field data [*Lippmann and Bodvarsson*, 1983*b*]. The single most important reservoir parameter controlling the steady state distribution of temperature and pressure in the system is the permeability. The permeability values were changed for the different cases studied, and it was found that the best match between computed and observed temperature values were obtained when the permeability anisotropy (k_{hor}/k_{vert}) in zones 1, 3, and 5 was kept at 10 and in zones 2 and 4 at 100.

The anisotropic nature of the permeability of the different regions seems reasonable when one considers the general intercalation of sandstones and shales in the lithologic column at Heber. The lower anisotropy of zones 1 and 3 could be due to a higher density of vertical fractures/faults, perhaps the faults postulated within the upflow region. On the other hand, in zone 5, below the bottom of the deepest wells at Heber, the lower anisotropy could be related to a larger sandstone content. This is consistent with an apparent increase of sandstone abundance with depth reported by *Tansev and Wasserman* [1978].

The thermal conductivity of the materials is another important parameter that affects the steady state thermodynamic conditions computed. Since no values of thermal conductivity of the various formations at Heber are available, we assume a value of 2 W/m °K. This value seems reasonable for sandstone and shale. However, for the materials in zones 1 and 2 (shallow layers) a lower value is assigned (1.088 W/m °K) based on the average thermal conductivity reported by *Combs* [1971] for 40 samples from 150-m-deep wells drilled in the Imperial Valley. It should be emphasized that the thermal conductivity values assigned to the shallow zones (zones 1 and 2) are much more important than those assigned to deeper reservoir zones because of the conductive heat losses to the surface.

The distributions of temperatures and pressures in the system under steady state (i.e., natural) conditions are not dependent upon rock parameters such as the porosity, rock density, heat capacity, thermal expansivity, or compressibility, since these are storage-type parameters. However, these parameters will affect the results of the exploitation calculations. Only an incomplete set of porosity data is available; *Ershaghi and Abdassah* [1983] published wireline log-derived porosities for two unidentified Heber wells. Porosity varies between 0.1 and 0.5; generally decreasing with depth. To our knowledge no values for the other parameters for Heber rocks have been published.

In this study, rock compressibility and thermal expansion are neglected; rock density and heat capacity are assumed to be constant and independent of rock type (Table 1). The porosities used are in the range given by *Ershaghi and Abdassah* [1983], and those found in other geothermal fields of the Salton Trough [*Riney et al.*, 1980; *Lippmann and Bodvarsson*, 1983*a*].

The salinity of the Heber geothermal fluid is low, or around 14,000 ppm [*Ershaghi and Abdassah*, 1983; *Riess and Meiran*, 1983]. Because of its low salinity the geothermal fluid is assumed to be pure water; its density, viscosity, and compressibility are allowed to vary with temperature and pressure. The specific heat of the fluid is kept constant (4200 J/kg °K); its thermal expansivity is neglected.

Best Model

Only the model that best reproduces the reported temperature distribution and pressure gradient in the Heber system is presented here. Results of a sensitivity study on the results are

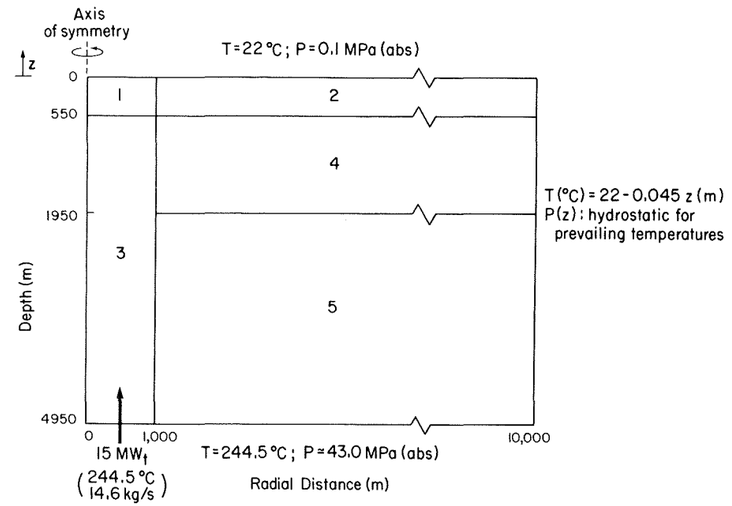

Fig. 4. Different zones and boundary conditions used in the (best) model. The upper and lower boundaries (except the bottom of zone 5) are closed to fluid flow and open to heat flow. The outer radial boundary is open to heat and fluid flow.

TABLE 1. Rock Properties Used in the Model

Zone	Porosity	Horizontal Permeability, 10^{-15} m^2	Vertical Permeability, 10^{-15} m^2	Conductivity Rock-Water Mixture, W/m °K
1	0.30	5	0.5	1.088
2	0.30	5	0.05	1.088
3	0.23	125	12.5	2.000
4	0.25	10	0.1	2.000
5	0.23	115	11.5	2.000

All rock parameters are assumed constant. Rock density and heat capacity are assumed to be uniform in the model, i.e., 2650 kg/m^3 and 1000 J/kg °K, respectively. Rock compressibility and thermal expansion are neglected.

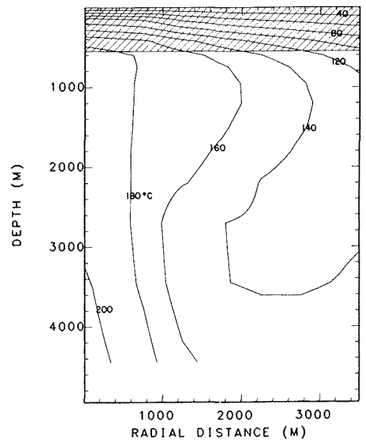

Fig. 5. Computed steady state temperature distribution. Hatched layer represents the cap rock (zones 1 and 2, see Figure 4).

discussed by *Lippmann and Bodvarsson* [1983*b*]. When evaluating the results, one should keep in mind that the radial model used in the simulations cannot replicate the horizontal groundwater flow which distorts the shape of the convective plume into a lopsided mushroom [*Salveson and Cooper*, 1981]. When matching values, the computed results were displayed as centered on well Nowlin 1 (Figure 3).

The best match between observed and computed values is obtained when the permeabilities and thermal conductivities given in Table 1 are used, and the recharge rate from below into the upflow zone (zone 3) is 14.6 kg/s of 244.5°C water, or equivalent to 15 MW thermal energy (reference temperature 0°C). The 244.5°C temperature at 4950 m depth corresponds to a geothermal gradient of about 45°C/km.

The computed temperature distribution in the system is shown in Figure 5 (only half of the cross section is depicted because of the axial symmetry of the model). Figure 5 shows that the isotherms above 160°C show the typical mushroom shape due to the outward flow of hot fluids in the upper part of the reservoir system and the inflow of colder fluids below. Consequently, one finds large temperature inversions in wells drilled outside the main upflow zone.

The comparison between observed and calculated temperatures is shown in the cross section given in Figure 6. The match obtained is reasonable when one considers the axial symmetry used in the simulations. The calculated isotherms are symmetrical, whereas the observed data show some nonsymmetrical behavior, probably due to regional groundwater flow and variations in the permeability distribution in the various reservoir regions. Figure 6 shows that the calculated isotherms spread too far to the SE in the upper regions of the reservoir but not far enough to the NW. Similarly, the calculated temperature inversions are too large in the lower part of the reservoir to the SE but are less than those observed to the NW. Overall, the computed temperature distribution approximately matches the observed one, so the actual energy input into the system is probably similar to that used in the simulation.

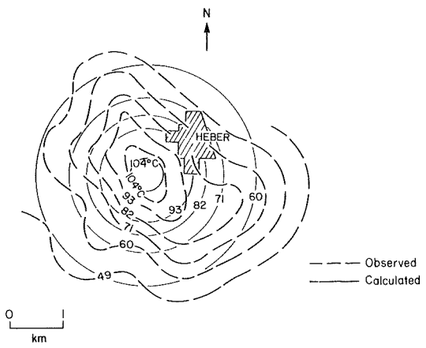

Fig. 7. Comparison between observed temperatures at 146 m depth [from *Salveson and Cooper*, 1981] and computed steady state temperatures at 150 m.

Figure 7 shows the comparison between observed shallow temperatures (146 m depth) reported by *Salveson and Cooper* [1981] and our calculated values at 150 m. The agreement is reasonable, indicating that heat losses to the surface are adequately modeled.

The computed pressure distribution in the upper 3000 m of the upflow zone is shown in Figure 8. The match with the observed pressure gradient (9.5 MPa/km) is good. The overall gradient from the ground surface to 1200 m depth is 9.82 MPa/km; to 1800 m, 9.54 MPa/km; and to 3450 m, 9.32 MPa/km. Thus, on the average, the calculated pressure gradient is very close to the observed value.

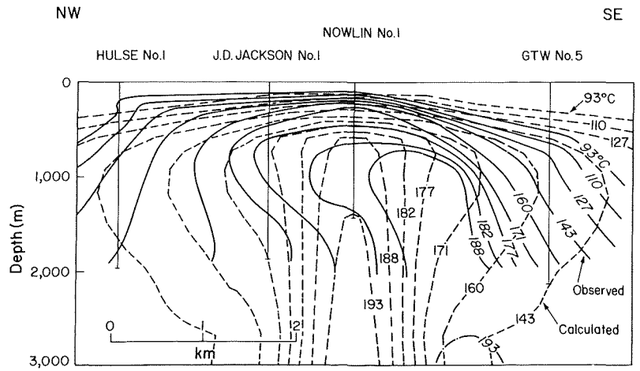

Fig. 6. Comparison between observed and computed steady state temperature distributions (see Figures 3 and 5.)

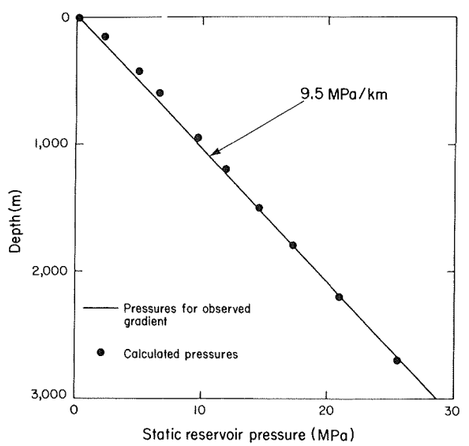

Fig. 8. Comparison between pressures computed based on the reported gradient and those calculated near the axis of the (best) model.

The computed flow patterns are shown in Figure 9. Hot water from the convective heat source ascends through the central upflow region (zone 3) and spreads laterally outward into the upper part of the system. Colder water surrounding the geothermal anomaly, because of its higher density, flows inward toward the upflow zone. This cold water inflow is slowed down significantly by the relatively low permeability of the upper outer region (zone 4). This is indicated by the blank zone in Figure 9. The length of the arrows is scaled with respect to the largest mass flow rate computed in the system. In the more permeable, deeper outer zone (zone 5) the cold water is more mobile and moves more rapidly toward the upflow zone. Near the bottom of the system, the high pressures created by the fluids recharging the upflow zone cause gradual outward fluid movement. Some fluid mixing occurs in the bottom of the upflow zone, reducing the temperature of the upwelling water.

The influx of colder water from regions outside the main geothermal anomaly creates the marked reversals of temperature in the outer regions of the system (Figure 5). This model seems to indicate that the so-called cap rock (zones 1 and 2) is quite permeable (5×10^{-15} m^2). If during the simulation its permeability is decreased significantly, the shallow temperatures (150 m depth) would drop below those reported by *Salveson and Cooper* [1981]. The match between observed and calculated cap rock temperatures could be improved by further decreasing the thermal conductivity of zones 1 and 2. However, for the cap rock a thermal conductivity value below 1 W/m °K seems unrealistic.

The horizontal permeability of the upper outer regions of the field (zone 4) seems very low (10×10^{-15} m^2) when one considers the relatively high horizontal permeability in the upflow zone (125×10^{-15} m^2). However, if we use a significantly larger permeability in this zone, the inflow of cooler fluids from the outside floods the system and causes much greater temperature reversals than those observed. The low permeability of this predominantly sandy zone could be explained either by the precipitation of silica in the rock pores as the geothermal waters flow outward and cool or by the precipitation of carbonates from the heating of cold water during the evolution of the system.

The conductive heat losses at the surface are significantly lower than those to the upper outer radial boundary where both conductive and convective losses occur. The surface heat losses for the central 1-km-radius circle amount to 1.75 MW (reference temperature 0°C; equivalent to 13.3 HFU (μcal cm^{-2} s^{-1}); for the 3-km circle, 8.63 MW (7.3 HFU); and for the entire 10-km-radius system, 36.6 MW (2.8 HFU). Heat is not only recharged at the bottom of the upflow zone via the 15-MW thermal convective source but also through fluid inflow from the outer radial boundary and conduction from below.

Modeling the Response to Exploitation

In the exploitation studies we use the same multilayer axisymmetric model, as in the natural state simulations. The rock properties of the different reservoir regions and the boundary conditions used are those determined by the natural state model. However, instead of prescribing a constant mass and energy flux into the system through the bottom of the 1000-m-radius upflow zone, as we did in the natural state model, we allow pressure-dependent recharge from a node (at a depth of about 5 km) with a constant temperature and pressure of 244.5°C and 45.67 MPa, respectively. Under natural state conditions this approach results in a mass recharge through the lower part of the upflow zone equal to 14.6 kg/s as in the best model of the natural system. During the simulation of the exploitation of the field, this rate of recharge will increase with time as the reservoir pressure in the upflow zone decreases. Thus, in general, the modeling of the upflow zone using a constant pressure boundary is an optimistic assumption, but we found that in our case it has only minor effects on the overall response of the system. The initial temperature and pressure conditions used in simulating the exploitation of the field correspond to those of the natural state model.

The main objective of this study is to find out what fluid extraction rates (i.e., generating capacity) are possible at Heber for different production-injection scenarios. It is assumed that

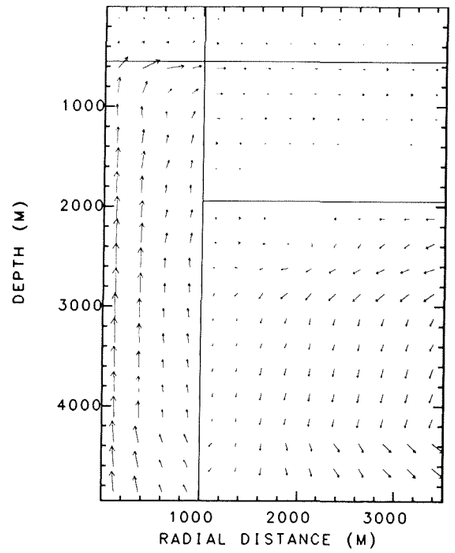

Fig. 9. Computed steady state mass flow pattern (length of arrows is scaled with respect to the largest computed mass flow rate).

TABLE 2. Reservoir Development Plans Studied for the Heber Field

Case	Production/Injection Depth Intervals, m	Average Radial Distance to Injection Zones, m
1 and 5	650–2950	2250
2 and 6	650–2950	4250
3	1950–2950	2250
4	1950–2950	4250

In all cases, fluid is produced from a 1000-m-radius axial cylinder.

during a 10-year period the installed generating capacity in the field increases linearly with time, from 0 MW_e at $t = 0$ to a maximum value at 10 years. From then on, the electrical power generation remains constant at the maximum level.

The simulations are carried out to 100 years or until boiling is observed in some part of the system (this always occurs in the shallow reservoir region near the axis). When boiling occurs, the reservoir pressure at the upper part of the production zone (at 750 m depth in cases 1 and 2) has generally dropped about 4 MPa; a drawdown considered to be excessive for a pumped system like that planned at Heber. On the basis of the published data noted above, it is assumed that 1000 kg/s of geothermal fluids are required to generate 50 MW_e.

Fluids are produced uniformly from part of the 1000-m-radius upflow zone (zone 3). In two of the six cases studied (Table 2, cases 1 and 2), production is uniformly distributed between 650 and 2950 m depth; the plan is similar to that described by *Salveson and Cooper* [1981]. In cases 3 and 4 the production is assumed to be restricted to deeper formations

TABLE 3. Production Characteristics After 40 Years

Fluid Production Rate, kg/s	Generating Capacity, MW_e	Reservoir Pressure,* MPa	ΔP, MPa	Average Temperature of Produced Fluids, °C	$\Delta \bar{T}$, °C
		Case 1			
4,000	~200	5.55	−2.31	168.0	−10.7
5,000	~250	4.93	−2.94	165.8	−12.9
6,000	~300	4.28	−3.59	163.6	−15.1
7,000†	~350	...	...	...	...
		Case 2			
2,000	~100	5.91	−1.96	172.7	−6.0
3,000	~150	4.91	−2.96	170.1	−8.6
4,000‡	~200	...	...	...	...
		Case 3			
6,000	~300	23.46	−1.97	144.1	−33.6
10,000	~500	21.74	−3.70	126.8	−51.0
		Case 4			
3,000	~300	24.24	−1.20	159.2	−18.5
10,000	~500	21.27	−4.17	146.0	−31.8
		Case 5			
6,000	~300	10.92	+3.05	160.9	−17.3
10,000	~500	12.86	+4.99	154.2	−24.0
		Case 6			
3,000	~150	7.82	−0.05	166.1	−12.1
5,000	~250	7.77	−0.10	161.5	−16.7
10,000	~500	7.62	−0.25	154.7	−23.5

*For cases 1, 2, 5, and 6, reservoir pressures correspond to the production node at $r = 100$ m and $z = -750$ m; for cases 3 and 4, to the node at $r = 100$ m and $z = -2700$ m.
†Boiling occurs in the system at about 25 years.
‡Boiling occurs in the system at about 12 years.

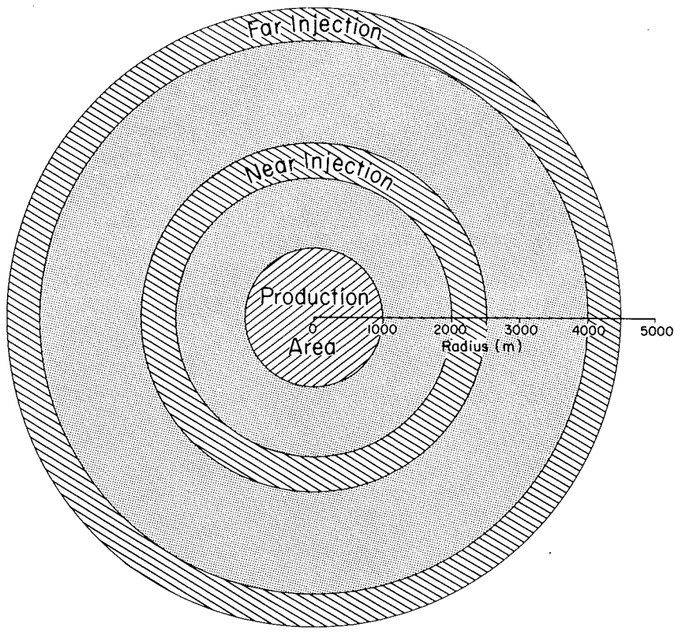

Fig. 10. Plan view of the production/injection model used for Heber.

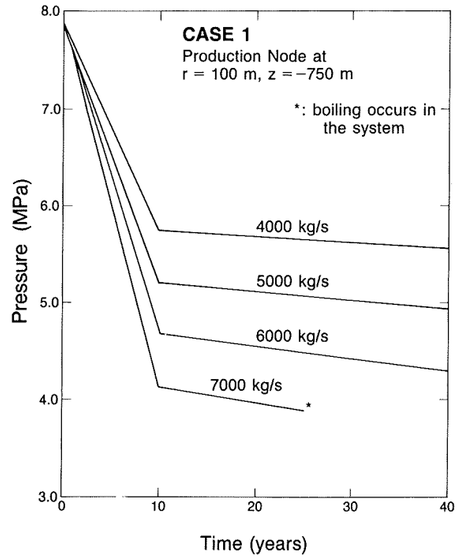

Fig. 11. Case 1. Pressure in production node at $r = 100$ m, $z = -750$ m.

(the 1950- to 2950-m-depth interval) facing the higher-permeability zone 5 (Figure 4). Finally, cases 5 and 6 evaluate an intermediate situation. Twenty-five percent of the produced fluids are extracted from the shallower depth interval (650–1950 m) and 75% from the deeper one (1950–2950 m).

One hundred percent of the fluids extracted from the reservoir are reinjected. In cases 1–4 at each depth interval the same mass of fluid is injected as is produced. In cases 5 and 6, 75% of the extracted fluids are injected into the upper depth

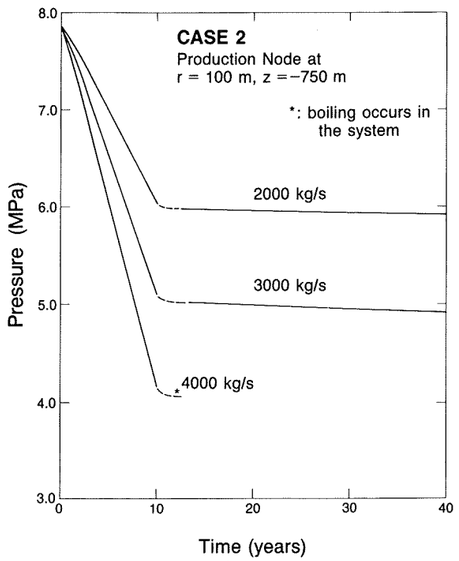

Fig. 12. Case 2. Pressure in production node at $r = 100$ m, $z = -750$ m.

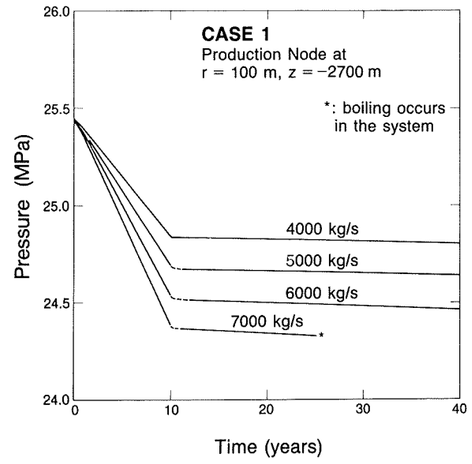

Fig. 13. Case 1. Pressure in production node at $r = 100$ m, $z = -2700$ m.

interval (650–1950 m) and 25% into the deeper one (1950–2950 m).

Reinjection is considered at several radial distances from the axis of the system (Figure 10). Two extreme situations are discussed here: (1) near injection, the uniform injection into an annular region extending between 2000 and 2500 m from the axis (cases 1, 3, and 5), and (2) far injection, the uniform injection into an annular region extending between 4000 and 4500 m from the axis (cases 2, 4, and 6). These two extremes bound the radial distances indicated by *Salveson and Cooper* [1981] for the location of the injected zones, i.e., 2.4–4.0 km. Following *Allen and Nelson* [1983, Figure 1] it is assumed that the injected fluid has a temperature of 72.2°C.

Results

Six possible reservoir development cases are discussed (see Table 2). The production characteristics after 40 years of de-

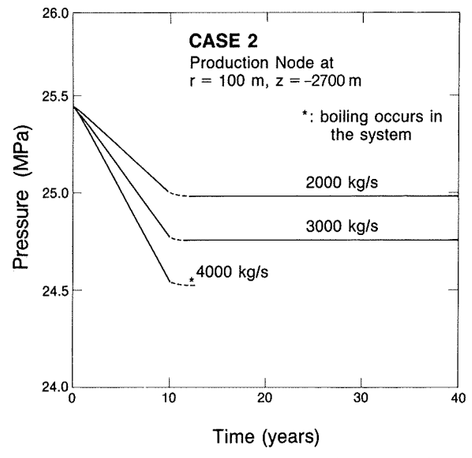

Fig. 14. Case 2. Pressure in production node at $r = 100$ m, $z = -2700$ m.

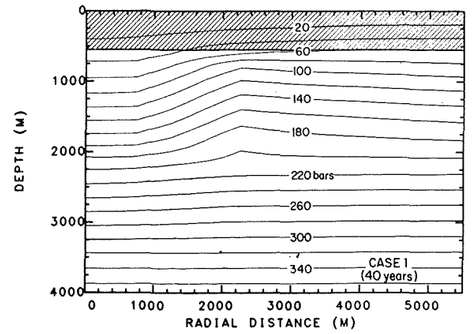

Fig. 15. Case 1. Computed pressure distribution in the system after 40 years of exploitation. Hatched region represents the cap rock.

velopment for all cases studied are summarized in Table 3.

Reservoir Pressures. The shape of the pressure versus time graphs for the production nodes (Figures 11–14) reflects the assumed field development plan. During the first 10 years the total production rate increases linearly with time, from zero to a maximum rate at 10 years. This causes a large pressure decline at early times. Later on, pressures tend to stabilize due to the constant extraction rate and also because of the 100% injection.

This linear behavior of the pressure curves reflects the effects of a line sink and a distant line source whose strengths initially increase linearly with time ($q = a + bt$; $t \leq t_1$) and then become constant ($q = a + bt_1$; $t > t_1$). Assuming isothermal conditions and neglecting the effects of partial penetration, one can derive the estimated pressure decline in the production area under the assumed reservoir development plan:

$$\Delta P(r_1, r_2, t) = \frac{\mu}{4\pi kh}\left\{\left(a + bt + \frac{r_1^2}{4\alpha}b\right)E_1\left(\frac{r_1^2}{4\alpha t}\right) - bt\exp\left(-\frac{r_1^2}{4\alpha t}\right) + \left(dt^* + \frac{r_1^2}{4\alpha}d\right)E_1\left(\frac{r_1^2}{4\alpha t^*}\right) - dt^*\exp\left(-\frac{r_1^2}{4\alpha t^*}\right)\right.$$

$$\left. - \left(a + bt + \frac{r_2^2}{4\alpha}b\right)E_1\left(\frac{r_2^2}{4\alpha t}\right) + bt\exp\left(-\frac{r_2^2}{4\alpha t}\right) - \left(dt^* + \frac{r_2^2}{4\alpha}d\right)E_1\left(\frac{r_2^2}{4\alpha t^*}\right) + dt^*\exp\left(-\frac{r_2^2}{4\alpha t^*}\right)\right\} \quad (1)$$

where

$$d = -\frac{a + bt_1}{t_1}$$

$$t^* = t - t_1 \qquad t^* > 0$$

$$E_1(z) = \int_z^\infty \frac{e^{-t}}{t}\,dt \qquad |\arg z| < \pi$$

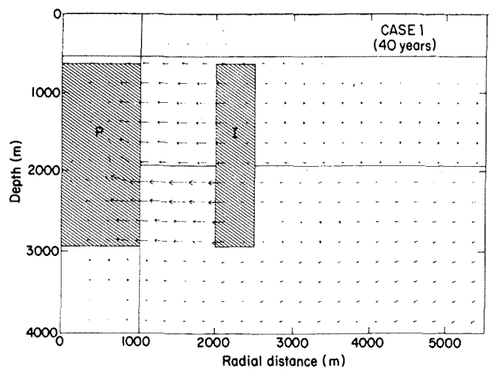

Fig. 16. Case 1. Computed mass flow pattern in the system after 40 years of exploitation. Length of arrows is scaled with respect to the largest mass flow rate. Lines delimit the different zones in the model. The hatched region represents the production (P) and injection (I) regions.

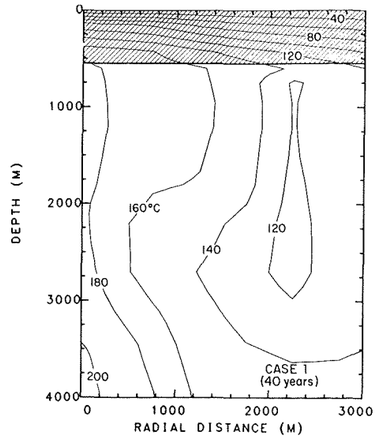

Fig. 17. Case 1. Computed temperature distribution in the system after 40 years of exploitation. Hatched region represents the cap rock.

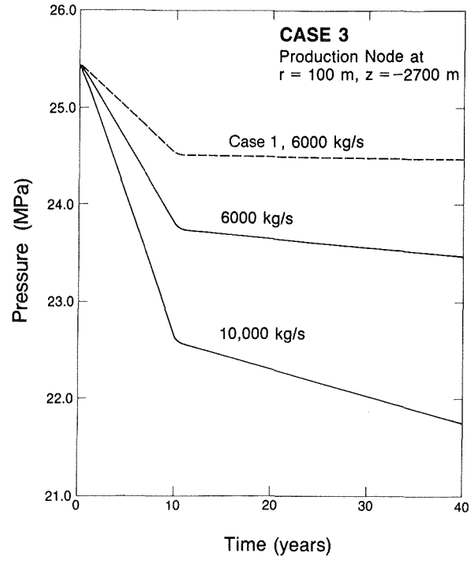

Fig. 18. Case 3. Pressure in production node at $r = 100$ m, $z = -2700$ m.

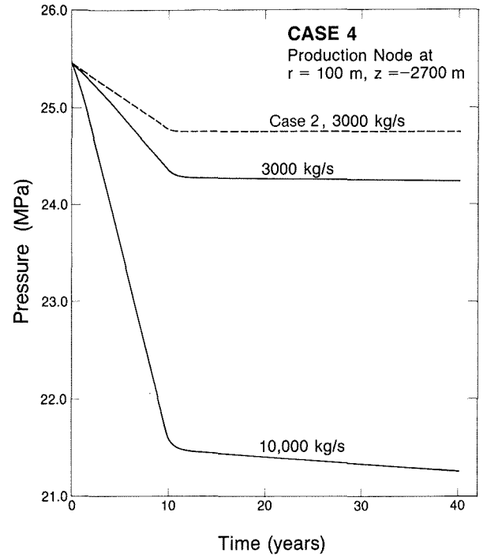

Fig. 19. Case 4. Pressure in production node at $r = 100$ m, $z = -2700$ m.

All of the symbols are defined in the notation section. Equation (1) is derived analytically using the Theis solution [*Theis*, 1935] and superposition principles.

Assuming at all times equal volumetric injection and production flow rates (q) and using parameters representative of our Heber study, the analytical solution indicates that the pressure in the production region should be practically constant after 10 years. However, in our case, the volumetric injection rate is smaller than the production rate because of the higher density of the injected water, explaining the gradual (linear) pressure drop for $t > 10$ years.

In cases 1 and 2 the drawdown in the upper part of the produced interval (Figures 11 and 12) is much larger than that in the lower part (Figures 13 and 14). This is mainly due to the limited fluid recharge to the shallower zones of the production region. In the upper part of the production zone the lateral recharge is limited because of the relatively low horizontal permeability (10×10^{-15} m^2) of zone 4. In comparison, for the lower part of the production zone the horizontal permeability of the neighboring zone 5 is 115×10^{-15} m^2. The effect of the permeability distribution on the pressure drop in the reservoir is evident in Figure 15, which shows pressure contours for case 1 after 40 years of exploitation. The effect of permeability contrast is also evident in the magnitude of the recharge to the different regions of the production zone, as illustrated in Figure 16; the length of the arrows is proportional to the mass flow rate. The influx of cooler fluids replacing hotter produced fluids and the cold water injection cause a rapid cooling of the reservoir. This is evident when one compares Figures 5 and 17.

In order to circumvent the effect of the lower permeability zone 4, in cases 3 and 4 the production and injection was restricted to the 1950- to 2950-m-depth interval (Table 2). In these cases, even though the fluid extraction rate per unit volume of production zone has more than doubled with respect to cases 1 and 2, less drawdown is observed. No boiling occurs in the system even when the production rate is as high as 10,000 kg/s (Figures 18 and 19).

In the final cases studied we assume 25% production and 75% injection from/into the shallower zone (between 650 and 1950 m) and 75% production and 25% injection from/into the deeper zone (1950–2950 m). The purpose of this case is to attempt to limit the pressure decline in the shallow production zone. As expected, in cases 5 and 6 the pressure does not drop as fast as in cases 1 and 2; it actually increases in case 5 (Table 3). However, the difficulty with this reservoir development plan is that the pressures in the injection region, because of the relative low permeability of zone 4, rise to excessive levels. For case 5 ($Q = 6000$ kg/s) at the end of the 40-year period the pressure in the injection node located at $r = 2250$ and 750 m depth has risen 7.60 MPa to 15.33 MPa (compare with case 1, Figure 20). The injection pressure for case 6 ($Q = 5000$ kg/s) is also high; that is, at $r = 4250$ and 750 m depth the pressure rises to 12.85 MPa, an increase of 5.23 MPa; for case 6 ($Q = 3000$ kg/s), $\Delta P = 3.13$ MPa. This suggests that most of the fluids must be injected into the deeper, more permeable zone.

The reservoir pressure support of the reinjection operations is clearly evident when one compares, e.g., the 4000 kg/s examples for cases 1 and 2 (Figures 11–14). The closer to the production zone that injection takes place, the greater is the pressure support. However, if fluids are injected too close to the production region, detrimental decreases in the temperature of the produced fluids may occur (see below).

The pressures in the injection nodes located in zone 4 are illustrated in Figure 20 (for cases 1 and 2). There is a rapid rise in pressure as the injection (and production) rate increases during the first 10 years. From then on, as the rate is kept constant, the pressure stabilizes (case 1) or even slowly decreases (case 2). On the other hand, the pressure in the injection nodes located in the higher permeability zone (zone 5) only changes slightly with time. For example, in case 4 (far injection) the total pressure rise after 40 years of injection at a rate of 10,000 kg/s is 0.35 MPa.

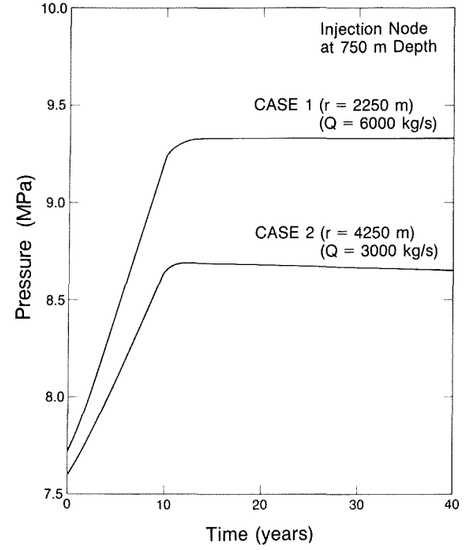

Fig. 20. Cases 1 and 2. Pressure in injection node at 750 m depth.

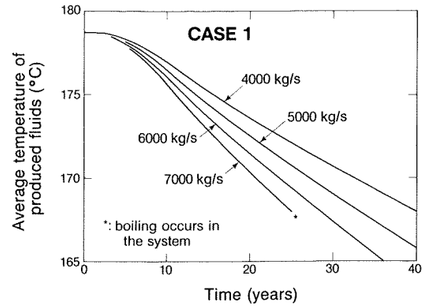

Fig. 21. Case 1. Average temperature of produced fluids.

Average production temperature. The temperatures reported here are the average temperatures of the produced fluids at the reservoir level. To obtain the temperature of the fluids at the inlet to the power plant, one must consider the heat losses in the well bore and also those in the surface hot water transmission pipes.

With production uniformly distributed over the 1000-m-radius cylinder the initial average temperature of the produced fluids (weighted by mass) is 178.7°C for cases 1 and 2, 177.8°C for cases 3 and 4, and 178.2°C for cases 5 and 6. Because of the characteristic mushroom shape of the isotherms in the reservoir (Figure 5) these average initial temperatures would be a few degrees higher if production is increased toward the axis of the system and correspondingly reduced if increased in the outer regions of the production cylinder. The changes in average fluid production temperatures with time for the first four cases are given in Figures 21–24. For most of the cases studied, the temperature decline of the produced fluids is entirely due to the inflow of colder fluids into the production area from the outer regions of the system but not due to the injection. This is evident when we compare the temperature decline for near and far injection cases (Table 3). However, in case 3, temperature decline due to the injected fluids is observed (compare Figures 23 and 24), which is partly due to the higher extraction/injection rates employed. Note that in our studies we do not model in detail the layering of sandstones and shales; hence the breakthrough times could be shorter than what we predict.

As one would expect from the production-injection scheme of cases 5 and 6, the temperature of the produced fluids fall between those of cases 1 and 2 and cases 3 and 4 (Table 3).

For most cases the temperature of the produced fluids is not significantly affected if the temperature of the injected fluids is increased slightly (e.g., 100°C instead of 72.2°C). For example, in case 1 (6000 kg/s) the average temperature after 40 years only increases from 163.6° to 163.9°C. However, because 100°C fluids have significantly lower viscosity than 72.2°C fluids, injection of higher-temperature fluids is preferred for pressure support. In case 1 (6000 kg/s) the 100°C injection delays the start of boiling in the system for about 12 years.

The Generating Capacity of the Field

In evaluating the generating capabilities of the field we must develop some criteria for maximum allowable pressure drop and temperature decline. The criteria we selected are as follows: (1) maximum allowable pressure drop is 4 MPa (corresponds to boiling starting in shallow zones), and (2) temperature of produced fluids must exceed 160°C, which is the economic fluid temperature limit for the power plant [*Tansev and Wasserman*, 1978]. Note, however, that we neglect heat losses during transport of the fluids in the well bore and surface pipes.

Most of the results show that the maximum extraction rates for the Heber reservoir are 6000 and 3000 kg/s for near and far injection, respectively. This corresponds to a power production of 300 and 150 MW_e, respectively. In cases 1 and 2 the limiting factor is the pressure drop in the reservoir, whereas in cases 3 and 4 the temperature decline limits the generating capacity. However, the results from case 6 indicate that optimum proportioning of the extraction/injection rates between different depth zones may enable 250-MW_e power production in the case of far injection. In this case one would expect large pressure increases due to injection in shallow regions.

Our results are more conservative than those of Chevron, the operator of the Heber field. They estimate a generating capacity of 500 MW_e (see the introduction), while our modeling study indicates a maximum of 300 MW_e. Because the details of their modeling effort are not in the public domain, we cannot directly compare our results to those of Chevron's. Our model shows that the relative low permeability of the upper outer zone (zone 4; 10×10^{-15} m^2 horizontal; 0.1×10^{-15} m^2 vertical) is the main limiting the factor for the generating capacity of the Heber field. This low-permeability zone was established from our modeling of the natural state of the system (see above). It is possible that recently completed wells at Heber may give a more optimistic temperature distribution than that shown in Figure 3. In that case the permeability of zone 4 (and the strength of the convective source) would be higher, thus increasing the maximum allowable generating capacity of the field.

CONCLUSIONS

Our simulation studies of the natural state of the Heber geothermal field indicate the following:

1. The upflow zone at Heber is a region of relatively high permeability (125×10^{-15} m^2 horizontal; 12.5×10^{-15} m^2 vertical). In this zone, hot waters upwell from depth and ascend to shallower layers where they spread laterally. At depth, colder waters move laterally into this zone and mix with the hot recharged waters.

2. The strength of the convective heat source is equivalent to about 15 MW_t (megawatts thermal) (reference temperature 0°C). No speculations can be made on the nature of this heat source before more field data become available.

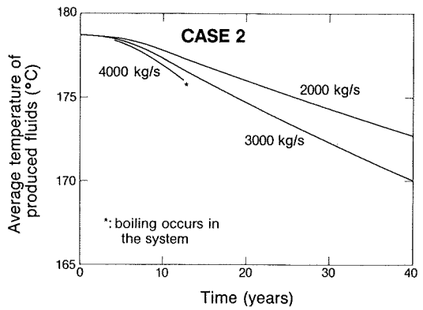

Fig. 22. Case 2. Average temperature of produced fluids.

3. Outside the central upflow zone, temperature reversals should be encountered by deeper wells.

4. The so-called cap rock is quite permeable (k horizontal $= 5 \times 10^{-15}$ m^2, k vertical $= 0.5$ to 0.05×10^{-15} m^2) at least in the lower part. This may suggest potential danger of cold fluid recharge from shallow regions.

5. The upper part of the outer region has a lower permeability (10×10^{-15} m^2 horizontal; 0.1×10^{-15} m^2 vertical) than the lower outer region. The original permeability could have been reduced by the precipitation of minerals in the pores of the rock matrix.

6. If one assumes a 40-year lifetime for the project, with 10 years to build up to the total electrical generating capacity and 30 years of maximum constant electrical power output, the results of our exploitation studies show that for injection between 2000 and 2500 m from the axis of the system (near injection) a maximum production rate of 6000 kg/s (about 300 MW_e) is possible. However, it should be stressed that in case 1, after 40 years of exploitation, the total pressure drop in the upper part of the produced region is about 3.6 MPa and the average temperature of the produced fluids (at reservoir level) will have declined about 15°C, to about 164°C. For case 3 the maximum possible mass extraction rate is below 6000 kg/s; for that rate after 40 years the production temperature would drop about 34°C, to about 144°C.

7. For injection between 4000 and 4500 m (far injection) the maximum feasible production rate is 3000 kg/s (about 150 MW_e). In case 2, after 40 years, the maximum drawdown in the reservoir (at $r = 100$ m, $z = -750$ m) is approximately 3.0 MPa and the average temperature of production fluids 170°C. In case 4 the pressure drop in the reservoir (at $r = 100$ m, $z = -2700$ m) is 1.2 MPa, and the temperature of the produced fluids will have dropped about 18°C, to about 159°C. The results from case 6 indicate a possible fluid production rate of 5000 kg/s (about 250 MW_e); however, large pressure increases in the injection zone are observed (about 5.2 MPa in the upper part).

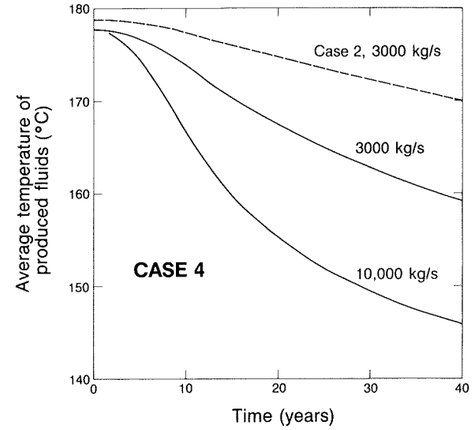

Fig. 24. Case 4. Average temperature of produced fluids.

NOTATION

a constant, m^3/s.
b constant, m^3/s^2.
d constant, m^3/s^2.
h aquifer thickness, m.
k intrinsic permeability, m^2.
P pressure, Pa.
Q mass flow rate, kg/s.
q volumetric flow rate, m^3/s.
r radial distance, m.
r_1 radial distance to production well, m.
r_2 radial distance to injection well, m.
T temperature, °C.
t time, s.
t_1 time after which strength of fluid source becomes constant, s.
$t^* = t - t_1$, s.
z elevation, m.
α diffusivity, m^2/s.
μ viscosity of fluid, Pa s.

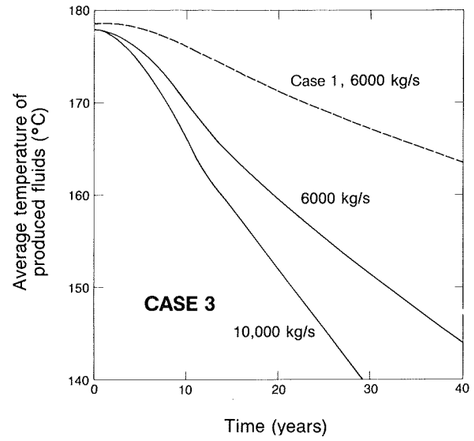

Fig. 23. Case 3. Average temperature of produced fluids.

Acknowledgments. We would like to thank our colleagues at the Lawrence Berkeley Laboratory, especially K. Pruess, C. Doughty, and J. Wang for reviewing the manuscript and for their suggestions. We also want to express our gratitude to the referees for their valuable comments on the draft. The assistance of P. Fuller and C. Doughty for the computer-generated graphs is appreciated. This work was supported by the Assistant Secretary for Conservation and Renewable Energy, Office of Renewable Technology, Division of Geothermal and Hydropower Technologies of the U.S. Department of Energy under contract DE-AC03-76SF00098. The views and opinions of authors expressed herein do not necessarily state or reflect those of the U.S. government or any agency thereof.

REFERENCES

Allen, R. F., and T. T. Nelson, Heber geothermal binary demonstration project, in *Proceedings of the Geothermal Program Review II*, pp. 235–241, U.S. Department of Energy, Washington, D. C., 1983.

Bodvarsson, G. S., Mathematical modeling of the behavior of geothermal systems under exploitation, *Rep. LBL-13937*, 353 pp., Lawrence Berkeley Lab., Berkeley, Calif., 1982.

Bodvarsson, G. S., K. Pruess, V. Stefansson, and E. T. Eliasson, Modeling studies of the natural state of the Krafla geothermal field, Proceedings of the Eighth Workshop Geothermal Reservoir Engineering, *Rep. SGP-TR-60*, pp. 211–217, Stanford Geotherm. Program, Stanford Univ., Stanford, Calif., 1982.

Bodvarsson, G. S., K. Pruess, V. Stefansson, and E. T. Eliasson, The Krafla geothermal field, Iceland, 2, The natural state of the system, *Water Resour. Res.*, *20*, 1531–1544, 1984.

Browne, P. R. L., Occurrence and hydrothermal alteration of diabase,

Heber geothermal field, Imperial Valley, California, *Rep. UCR/IGPP 77/9*, 67 pp., Univ. of Calif., Riverside, 1977.

Butler, D. R., Heber, Geothermal Development of the Salton Trough, California and Mexico, *Rep. UCRL-51775*, pp. 23–25, Lawrence Livermore Lab., Livermore, Calif., 1975.

California Division of Oil and Gas, Chevron, Dravo, may be partners in Heber dual flash project, *Geotherm. Hot Line*, *13*(1), 7–8, 1983*a*.

California Division of Oil and Gas, Heber power plant projects underway, *Geotherm. Hot Line*, *13*(2), 50–51, 1983*b*.

Combs, J., Heat flow and geothermal resource estimate for the Imperial Valley, in *Cooperative Geological-Geophysical-Geochemical Investigations of Geothermal Resources in the Imperial Valley Area of California*, edited by R. W. Rex et al., pp. 5–27, University of California, Riverside, 1971.

De Haven, N. J., Heber geothermal project, *Geotherm. Resour. Counc. Trans.*, *6*, 339–341, 1982.

Edwards, A. L., TRUMP: A computer program for transient and steady-state temperature distribution in multidimensional systems, *Rep. UCRL-14754, Rev. 4*, 259 pp., Lawrence Livermore Lab., Livermore, Calif., 1972.

Duff, I. S., MA28—A set of FORTRAN subroutines for sparse unsymmetric linear equations, *Rep. AERE-R 8730*, 153 pp., U. K. At. Energy Auth., Harwell, Oxfordshire, Great Britain, 1977.

Doughty, C., T. A. Buscheck, and C. F. Tsang, Prediction and analysis of a field experiment on a multilayered aquifer thermal energy storage system with strong bouyancy flow, *Water Resour. Res.*, *19*(5), 1307–1315, 1983.

Elders, W. A., and L. H. Cohen, The Salton Sea geothermal field, California, as a near-field natural analog of a radioactive waste repository in salt, *Rep. BMI/ONWI-513*, 138 pp., Office of Nucl. Waste Isolation, Columbus, Ohio, 1983.

Ershaghi, I., and D. Abdassah, Interpretation of some wireline logs in geothermal fields of the Imperial Valley, California, paper presented at 1983 California Regional Meeting, Soc. Pet. Eng., Ventura, Calif., March 23–25, 1983.

Fuis, G. S., W. D. Mooney, J. H. Healy, G. A. McMechan, and W. J. Lutter, A seismic refraction survey of the Imperial Valley region, California, *J. Geophys. Res.*, *89*(B2), 1165–1189, 1984.

Goyal, K. P., and D. R. Kassoy, A plausible two-dimensional vertical model of the East Mesa geothermal field, California, *J. Geophys. Res.*, *86*(B11), 10719–10733, 1981.

Imperial Irrigation District, Imperial Valley monthly high, low and mean temperatures and rainfall 1914–1977, Imperial Irrig. Dist., Community and Spec. Serv., El Centro, Calif., 1978.

Lippmann, M. J., and G. S. Bodvarsson, Numerical studies of the heat and mass transport in the Cerro Prieto geothermal field, Mexico, *Water Resour. Res.*, *19*, 753–767, 1983*a*.

Lippmann, M. J., and G. S. Bodvarsson, A modeling study of the natural state of the Heber geothermal system, California, *Trans. Geotherm. Resour. Counc.*, *7*, 441–447, 1983*b*.

Riess, M. L., and P. F. Meiran, Design of the brine-hydrocarbon heat exchangers for the Heber geothermal binary demonstration power plant, *Trans. Geotherm. Resour. Counc.*, *7*, 35–40, 1983.

Riney, T. D., J. W. Pritchett, and L. F. Price, Integrated model of the shallow and deep hydrothermal systems in the East Mesa area, Imperial Valley, California, *Rep. SSS-R-80-4362*, 116 pp., S-Cubed, La Jolla, Calif., 1980.

Salveson, J. O., and A. M. Cooper, Exploration and development of the Heber geothermal field, Imperial Valley, California, paper presented at the 1981 New Zealand Geothermal Workshop, Univ. of Auckland, Auckland, N. Z., 1981.

Tansev, E. O., and M. L. Wasserman, Modeling the Heber geothermal reservoir, *Trans. Geotherm. Resour. Counc.*, *2*, 645–648, 1978.

Theis, C. V., The relationship between the lowering of piezometric surface and the rate and duration of discharge using ground-water storage, *Eos Trans. AGU*, *16*, 519–524, 1935.

G. S. Bodvarsson and M. J. Lippmann, Earth Sciences Division, Lawrence Berkeley Laboratory, 1 Cyclotron Road, Berkeley, CA 94720.

(Received March 30, 1984;
revised August 1, 1984;
accepted August 14, 1984.)